Tuning the aggregation of graphene oxide dispersions to synthesize elastic, low density graphene aerogels

*Kaiwen Hu [1], Thomas Szkopek [2 *] and Marta Cerruti [1*]*

[1]Department of Mining and Materials Engineering, McGill University, Montreal, QC, H3A 2B2, Canada.

[2]Department of Electrical and Computer Engineering, McGill University, Montreal, QC, H3A 0E9, Canada.

Supporting Information

This document contains

Additional experimental details (section 1)

Supporting figures (section 2)

Supporting tables and calculations (section 3)

1. Additional experimental details:

1.1 Thermogravimetric analysis

Thermo-decomposition of the GOs were monitored using a thermogravimetric analyzer (TA Instruments, USA) in air from room temperature to 900 °C at a heating rate of 20 °C min^{-1}. Isothermal TGA measurements were performed by ramping the temperature to the pre-annealing temperature at a heating rate of 20 °C min^{-1} followed by isothermal heating at the target temperature for 1 hour.

1.2 Acid-base titration

Potentiometric acid-base titrations of GO dispersions (0.62 mg·ml^{-1}, 20 ml) were performed by the addition of standard 0.0025 mol NaOH solution dropwise. All titrations were performed manually using a buret and a digital pH meter (Thermo Fisher Scientific, USA). The GO dispersion underwent constant stirring during the titration, and a stable pH value (>5 s) was recorded after each titrant addition.

1.3 X-ray photoelectron spectroscopy

X-ray photoelectron spectroscopy (XPS) of GOs and GAs were performed on a monochromatic Al K-Alpha photoelectron spectrometer (Thermoscientific, USA). At least three survey scans were collected between 0 and 1200 eV with a step size of 1 eV for each sample. Elemental high-resolution scans were performed with a step size of 0.1 eV and repeated at least 3 times. The peak fittings were completed with the software Thermo Avantage (version 5.9); spectral energies were calibrated by setting the C_{1s} binding energy as 284.8 eV. The spectra were deconvolved into four components, C−C (284.8 eV), C=O (288.2 eV), C-O (286.8 eV), and π−π* shake up (290.7 eV).

2. Figures

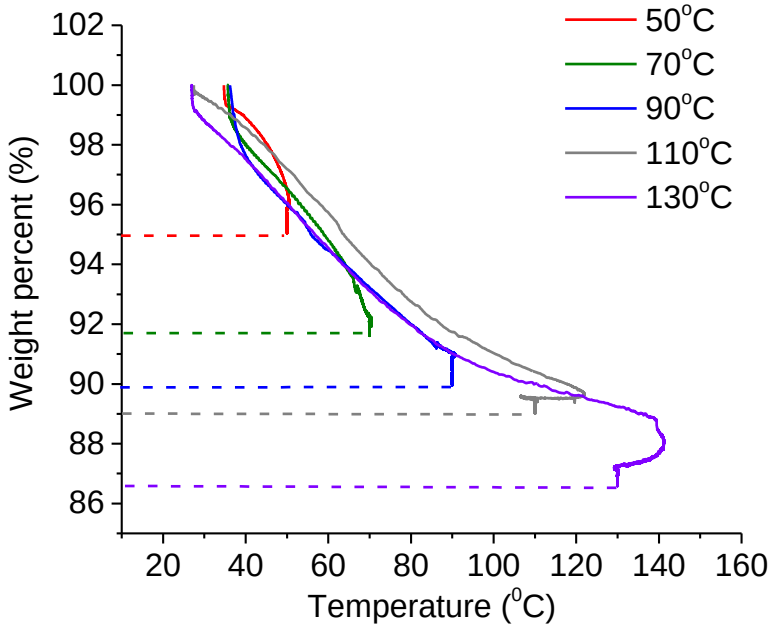

Figure S1. Mass loss profile of GO obtained from isothermal TGA at different temperatures showing the mass loss of GO during the annealing process

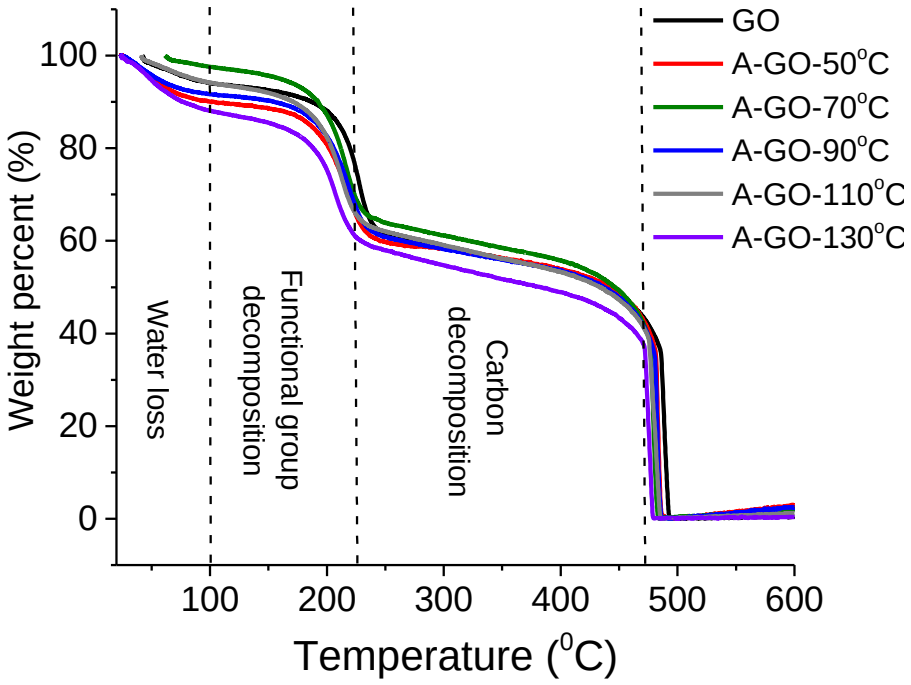

Figure S2. Mass loss profile of GO and A-GO obtained from ramped TGA

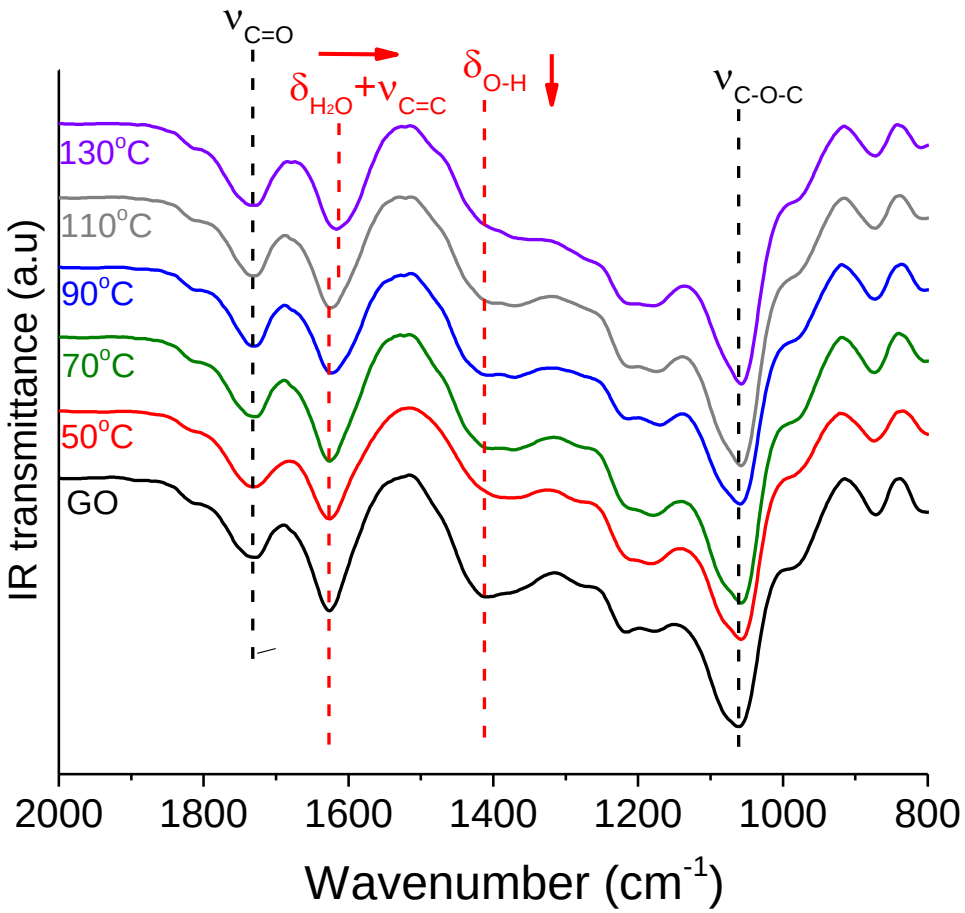

Figure S3. ATR-FTIR spectra of GO samples showing the red shift of δ_{H2O} and the decreased intensity of δ_{O-H}; The A-GOs showed two major differences in the fingerprint region: a decrease in the absorption of the δ_{O-H} peak at 1412 cm^{-1} [1,2], observed on all annealed GO samples, a decrease and a red shift of up to 12 cm^{-1} in the peak positioned at 1628 cm^{-1} upon annealing at 90 °C or higher. This peak is dominated by the water scissoring mode (δ_{H2O}) in GO [1-4]. The red shift of water scissoring bending is indicative of a slight change in hydrogen bonding energy [5,6]. These observations indicate that the low temperature annealing can remove some of the hydroxyl groups and intercalated water in GO while other functional groups such as carbonyls ($\nu_{C=O}$) and epoxides (ν_{C-O-C}) stay predominantly intact, as seen from the unchanged IR absorption at 1732 cm^{-1} and 1063 cm^{-1}

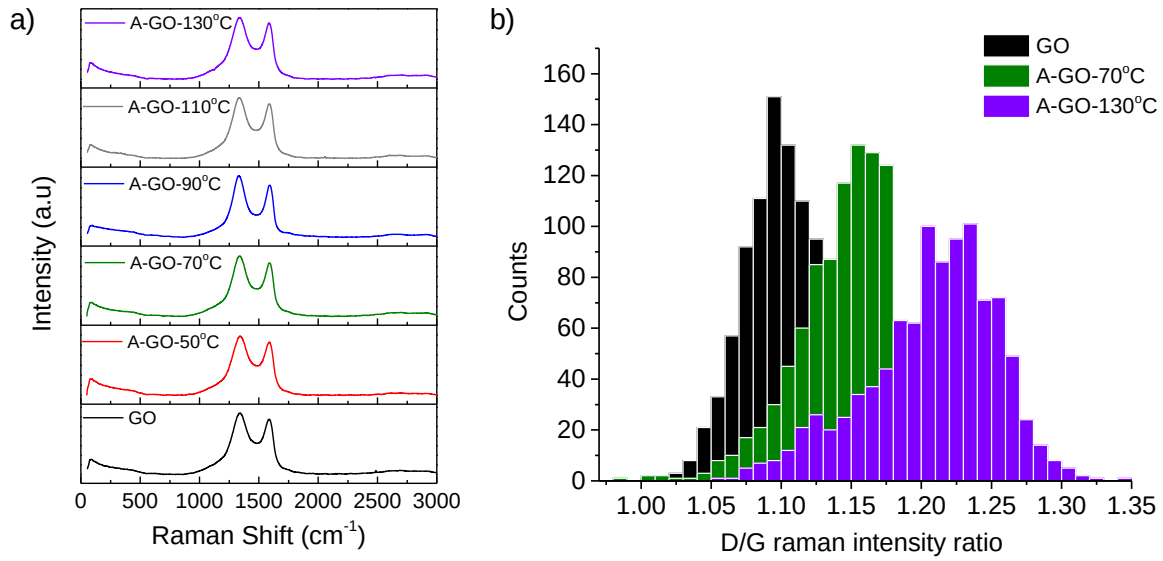

Figure S4. Raman spectra a) and statistical analysis b) of Raman mapping results of GO and A-GO; Raman spectra of annealed GO powders are similar to that of the original GO, with two prominent first order scattering peaks, namely the D band (~1340 cm^{-1}) and the G band (~1580 cm^{-1}), which are related to the C-C in plane stretching of graphitic carbon and the defect induced translational symmetry breaking [7]. All GO samples also showed second order scattering bands such as the G' band (~2700 cm^{-1}), which is a sensitive probe to perturbations of the sp^2 domains of graphene [7]. Conventionally, the Raman intensity ratio I_D/I_G can be used to quantify the mean distance between point defects (L_D) in graphene and its derivative materials [8-10]. Since the individual spectra of pristine and annealed GOs were very similar, we used Raman mapping to collect a statistical distribution of the I_D/I_G ratios [10] over 1000 points on each sample. Increasing the annealing temperature of GO resulted in a small upshift of the I_D/I_G ratio from 1.10 to 1.21 at 130 °C. Lucchese et al. [11] showed that I_D/I_G initially increases with increasing L_D, but decreases with L_D once L_D is larger than 3.5 nm. GO and rGO belong to the latter case (L_D > 3.5 nm) [8,9,12]. Therefore, the increase in the I_D/I_G ratio for annealed GO indicates a reduction in L_D and hence an increase in size of sp^2 domains. A broadened distribution of the I_D/I_G ratios was also seen for GO annealed at temperatures higher than 90 °C, indicating an increase in the heterogeneity of the sp^2 distribution [10]. This observation may be related to sp^2 clustering [12] or a slight thermal reduction [8,9] that could take place at higher annealing temperatures (> 90°C). However, the full width half maximum (FWHM) of the G' band of the GO samples (Supplementary **Table S1**) were all around 270 cm^{-1}, indicating that the observed decrease in defect density after annealing was minimal [8,9].

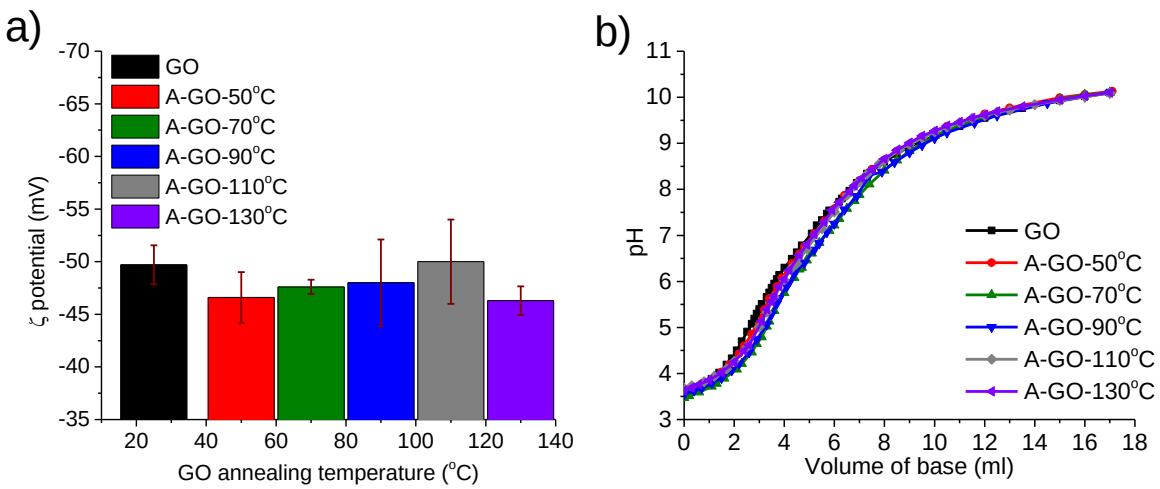

Figure S5. Zeta potential values a) and Potentiometric acid-base titration curves b) of GO and A-GO dispersions showing no significant change in the strength of electrostatic repulsion after the annealing.

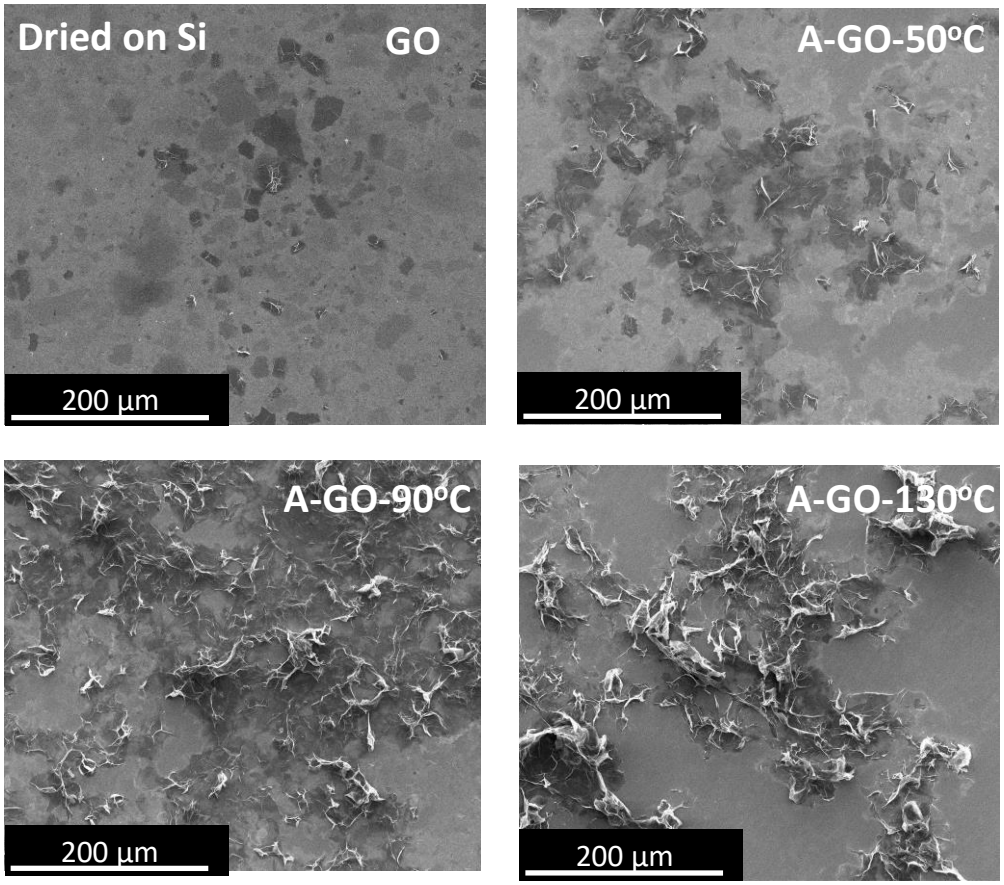

Figure S6. SEM images showing the morphology of GO sheets suspended on Si prepared by drop casting of ultra-dilute GO/A-GO dispersions (10 µg·ml^{-1}); while GO sheets remain flat A-GO sheets are wrinkled and folded

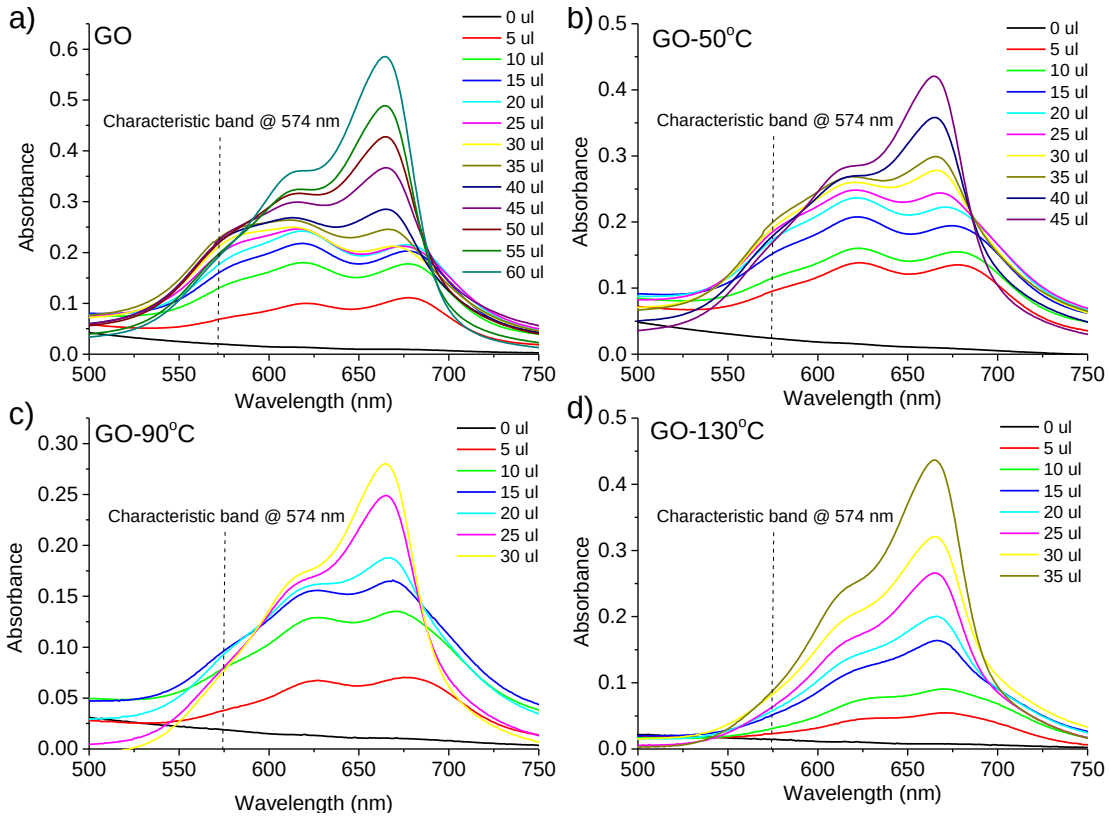

Figure S7. UV-vis absorption spectra of GO-MB dispersion and annealed GO-MB dispersions during MB titration; The characteristic band previously reported at 580 nm appears at 574 nm in our spectra, likely because of the slight difference in GO chemistry If a GO dispersion is titrated with MB, the 574 nm peak first increases in intensity, until saturation is reached. A further increase in MB concentration leads to a decrease in the band intensity, due to the precipitation of GO-MB aggregates; the absorption of the characteristic band at 574 nm saturated at lower MB amount at higher annealing temperatures and such saturation characteristic disappear at 130 ^{o}C due to significant loss of solvent exposed area of GO.

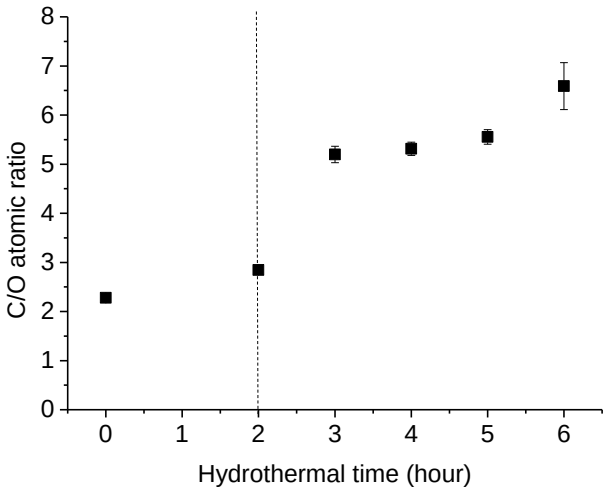

Figure S8. Evolution of C/O atomic ratio of the rGO during hydrothermal reduction; the C/O atomic ratios were calculated based on the atomic composition of XPS survey scans

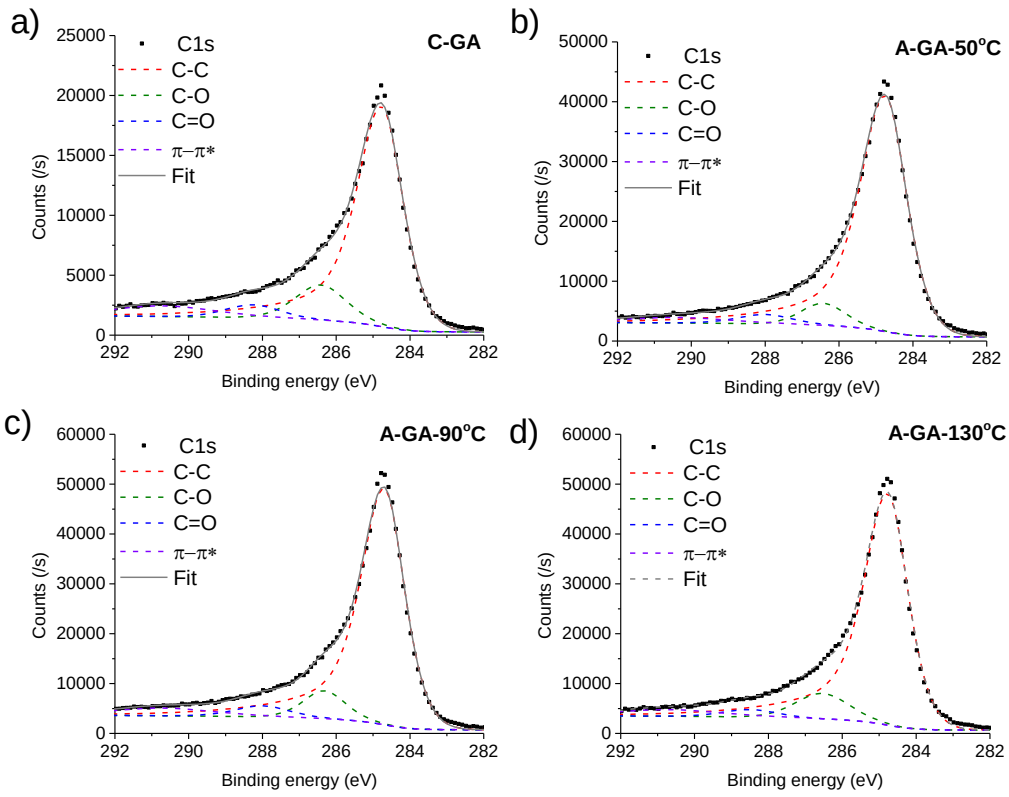

Figure S9. High resolution C_{1s} spectra of C-GA and A-GAs with deconvolution of the spectra into C-C, C-O, C=O and π-π* components

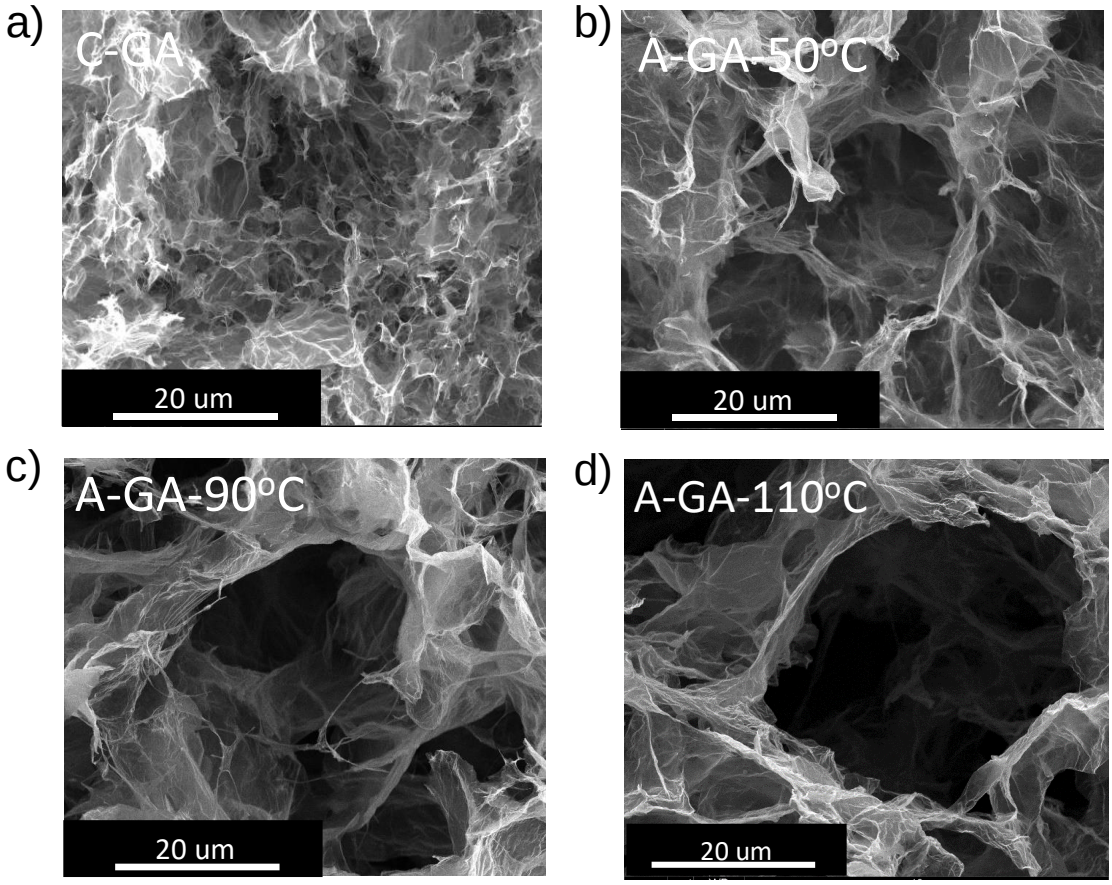

Figure S10. High magnification SEM images of C-GA and A-GAs showing their difference in porous structure; in a) C-GA had extended pore walls and the pores appeared to be smaller and more closed whereas A-GAs showed more open pore features with larger pore; From these high magnification SEM images, we found similar pore wall thicknesses for C-GA and A-GAs, which were both below 0.5 μm. For C-GA, thickening of pore walls mainly happened during the hydrothermal treatment and was driven by the strong hydrophobic attraction during the volume shrinkage stage. As for A-GAs, the stacking of pore walls mainly took place during the annealing step and was driven by the π-π stacking due to their large particle size and the decreased hydrophobic interaction

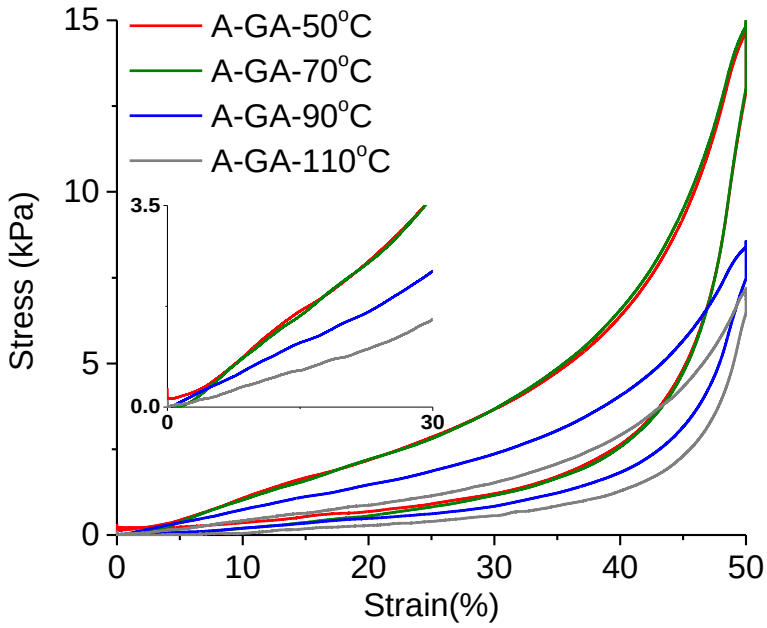

Figure S11. Stress-strain curves of A-GA prepared under different GO annealing temperatures at the 5th compression-release cycle; the young's modulus and the mechanical strength can be tuned by the annealing temperature; the inset shows that the compressive stresses of the aerogels at low strain are above zero; A-GAs showed negligible plastic strain as evidenced by the rising stress at low strain (<5%) 5 cycles. The shape of the stress-strain curves at different cycles were very similar, showing a long near linear elastic region up to about 35% strain, followed by a rapid increase in stress, indicative of densification. Unlike what observed for C-GAs, the quasi-plateau region of the stress-strain curve of A-GAs were not well distinguished from the linear elastic region. For elastic foams, the quasi-plateau region is a direct evidence of elastic buckling of the pore wall [13-16]. The lack of elastic buckling in the elastic deformation of A-GA were also observed in other elastic GA [14] and were previously ascribed to the high membrane stress of rGO pore walls. Here, the lack of plateau was likely due to the thick and wrinkled pore walls of the A-GAs, which originated from the π-π stacking of GO sheets during the mild annealing. Stiffer and stronger gels were produced at lower annealing temperatures, as expected due to their higher density. The compressive moduli of the A-GAs ranged from 5.0 GPa to 13.1 GPa after 5 cycles of compression.

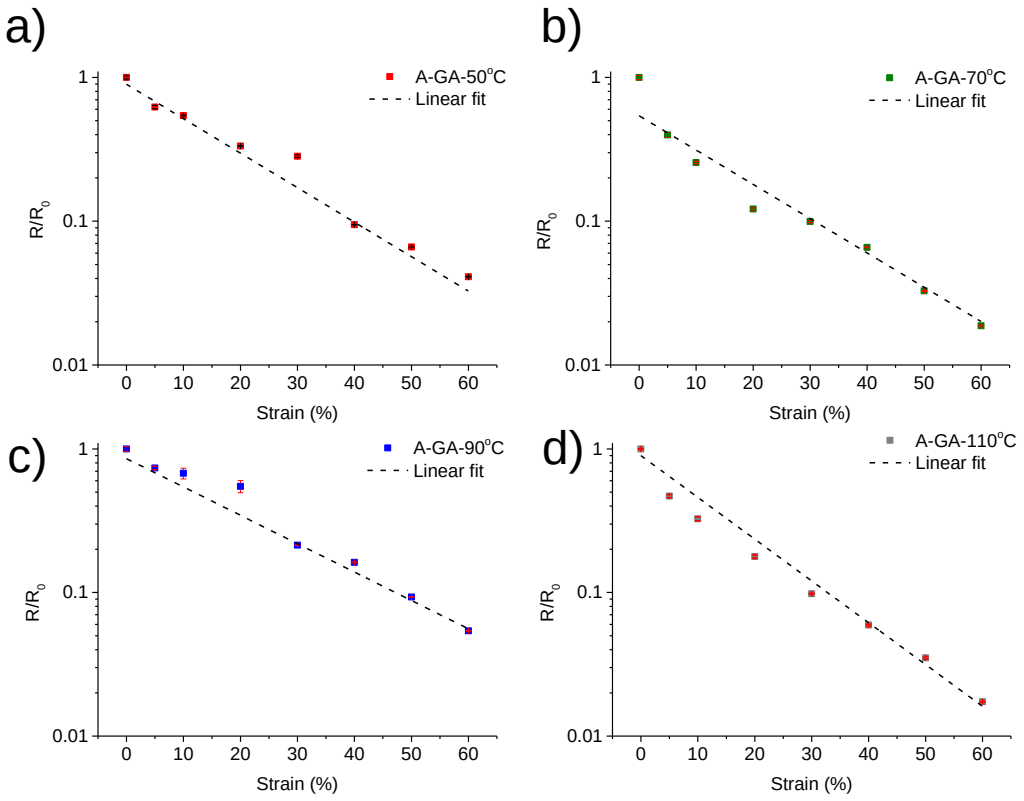

Figure S12. Resistance change vs. strain plot for different A-GAs showing more than 94% change upon compressing up to 60% strain; the resistance change followed a near linear response when plotted in logarithmic scale

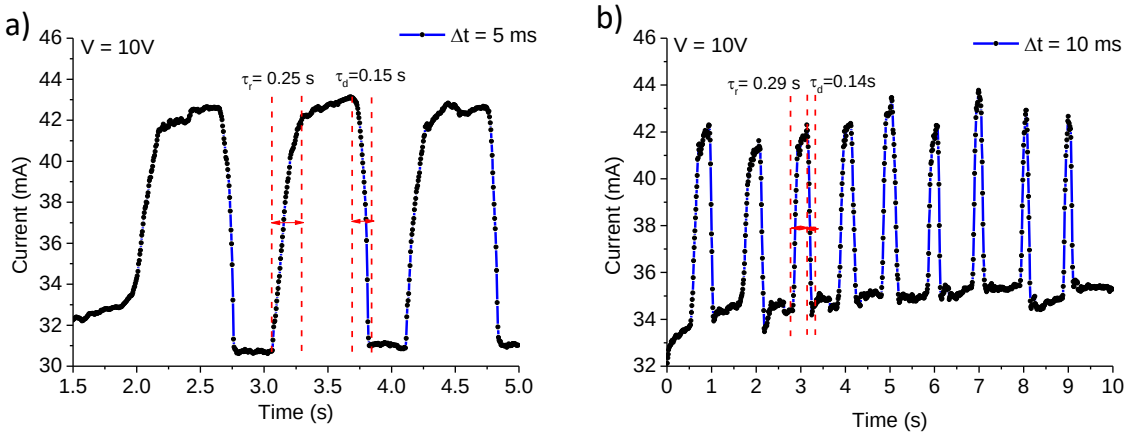

Figure S13. Current-time response during strain sensing measurements of A-GA-90°C with repeated step-like applied force profiles recorded: a) with a sampling time of Δt = 5 ms; b) and a longer recording with a greater number of cycles measured with a sampling time Δt = 10 ms. The rise response time (τ_r) and the decay response time (τ_d) of each compression-release cycle is shown. The response time is limited by the rate of mechanical compression and release rather than electrical response time. A typical mechanical release time is about 0.25 s, in good agreement with the τd measured in a) and b)

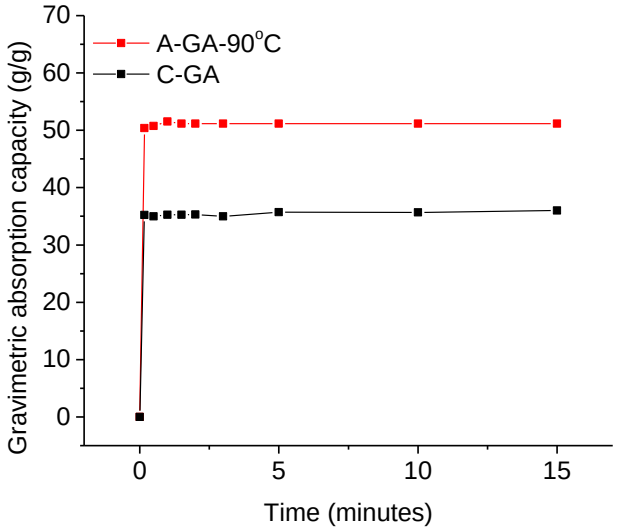

Figure S14. Hexane absorption capacity vs. time plot for C-GA and A-GA-90ºC showing their fast absorption kinetics; both GAs reached 98% of their absorption capacity of in less than 10 seconds

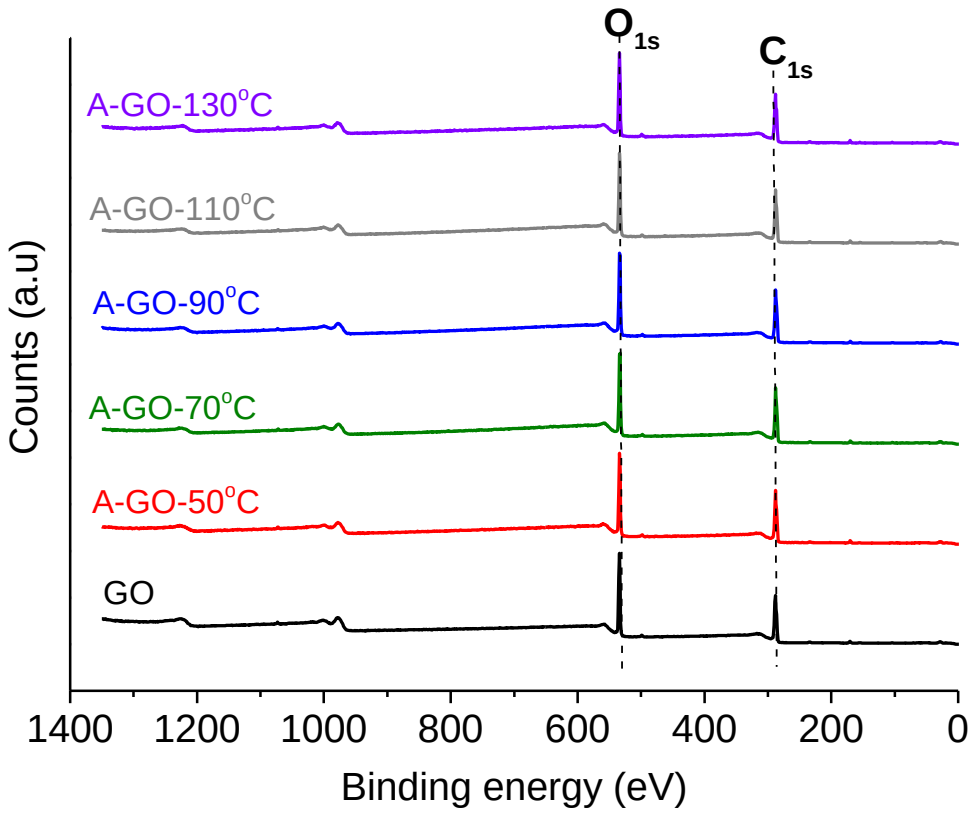

Figure S15. XPS survey spectra of GO and A-GO (50ºC-130ºC) showing minimum change in signal ratio of C_{1s}/O_{1s}

3. Tables and calculations

Table S1. Summary of C/O atomic ratio calculated based on XPS survey data, mass loss during annealing calculated by isothermal TGA measurements and I_D/I_G ratio and G' full width half maximum values of GO and annealed GOs from Raman results

Sample	C/O atomic ratio	Mass loss during annealing (wt%)	I_D/I_G ratio	G' FWHM (cm^{-1})
GO	2.14 ± 0.19	0	1.10 ± 0.03	279 ± 43
A-GO-50°C	2.03 ± 0.08	4.9	1.13 ± 0.03	286 ± 53
A-GO-70°C	1.97 ± 0.14	8.3	1.14 ± 0.03	N/A
A-GO-90°C	2.00 ± 0.03	9.7	1.21 ± 0.04	265 ± 13
A-GO-110°C	2.02 ± 0.02	11.0	1.25 ± 0.06	N/A
A-GO-130°C	2.01 ± 0.04	13.4	1.21 ± 0.05	276 ± 37

Table S2. XPS C_{1s} deconvoluted peak contributions of GO and A-GOs

Sample	C-C (%)	C-O (%)	C=O (%)	π-π* (%)
GO	46.3 ± 3.3	45.8 ± 2.8	7.5 ± 0.4	0.5 ± 0.1
A-GO-50°C	46.7 ± 1.4	43.8 ± 1.4	8.2 ± 2.1	1.3 ±0.7
A-GO-70°C	45.1 ± 1.6	46.0 ± 1.0	8.4 ± 0.4	0.5± 0.3
A-GO-90°C	45.7 ± 1.0	45.2 ± 1.3	8.0 ± 0.1	1.1 ± 0.5
A-GO-110°C	47.0 ± 0.7	44.3 ± 1.0	8.1 ± 0.7	0.6 ± 0.5
A-GO-130°C	46.6 ± 1.3	44.2 ± 1.2	8.1 ± 0.4	1.2 ± 0.4

Table S3. Summary of C/O atomic ratios of C-GA and A-GAs calculated based on XPS survey data

GA	C/O atomic ratio
C-GA	5.6 ± 0.3
A-GA-50°C	5.4 ± 0.7
A-GA-90°C	6.1 ± 1.5
A-GA-110°C	5.8 ± 0.5

Table S4. Summary of energy loss coefficients (δ) of C-GA and A-GAs; % loss was calculated based on the ratio between the loss of δ compared to the first cycle and the δ of the first cycle

GA	1st cycle δ (%)	5th cycle δ (%)	% loss
C-GA	93.0	51.7	44.4
A-GA-50°C	63.7	52.6	17.4
A-GA-70°C	62.2	55.7	10.5
A-GA-90°C	57.4	51.3 (48.6 at 20th)	10.6 (15.3 at 20th)
A-GA-110°C	56.7	51.5	9.2

Table S5. Summary of strain sensitivity (gauge factor) of A-GAs

GA	Sensitivity gauge factor (decade $\Delta(R/R_0)/\Delta\varepsilon$)
A-GA-50°C	-0.024
A-GA-70°C	-0.023
A-GA-90°C	-0.020
A-GA-110°C	-0.029
Ultralight EDA reduced GA [17]	-0.020
Based induced liquid crystal GA [13]	-0.006
Emulsion templated GA [14]	-0.003

Calculation of charge density of GO and annealed GO from acid-base titration:

First, the base consumption volume (V_b) for neutralization of GO acidity was estimated from the base consumption in **Figure S4** at the bending point around pH=9.5 [3].

The number of moles of base consumed for neutralization of GO (n_b) can be calculated by:

$n_b = N_A \times V_b$ Eq. 1

where N_A is the Avogadro number.

The acid group density (ρ_a) on GO can simply be calculated by Eq. 2:

$\rho_a = \frac{n_b}{m_{GO}}$ Eq. 2

Where m_{GO} is the mass of GO used in the titration

Finally, the charge density of GO is calculated by Eq. 3:

$\sigma_q = \frac{\rho_a \times F}{A_{GO}}$ Eq. 3

where F is the Faraday's constant and A_{GO} is the specific surface area of GO, which is 736.6 m^2/g [18].

Calculation of solvent exposed area of GO and annealed GO:

First, the saturation volume of MB solution (V_s) was obtained from **Figure S5** by finding the maximum absorption of the characteristic band of MB-GO at 574 nm. Multiplying V_s by the concentration of the MB solution, we get the number of moles of MB consumed (N_b). The solvent exposed area of GO (A_s) can thus be calculated from Eq. 4:

$$A_s = \frac{N_b \times M_{MB} \times A_{MB}}{m_{GO}} \quad \text{Eq. 4}$$

where M_{MB} is the molar mass of MB and A_{MB} is the surface coverage of MB on graphitic materials, which is 2.54 m^2/mg of MB [18].

References:

1 Hu, K., Xie, X., Szkopek, T. & Cerruti, M. Understanding hydrothermally reduced graphene oxide hydrogels: from reaction products to hydrogel properties. *Chemistry of Materials* **28**, 1756-1768 (2016).

2 Mungse, H. P., Sharma, O. P., Sugimura, H. & Khatri, O. P. Hydrothermal deoxygenation of graphene oxide in sub-and supercritical water. *RSC Advances* **4**, 22589-22595 (2014).

3 Dimiev, A. M., Alemany, L. B. & Tour, J. M. Graphene oxide. Origin of acidity, its instability in water, and a new dynamic structural model. *ACS nano* **7**, 576-588 (2012).

4 Eigler, S., Dotzer, C., Hirsch, A., Enzelberger, M. & Müller, P. Formation and decomposition of CO2 intercalated graphene oxide. *Chemistry of Materials* **24**, 1276-1282 (2012).

5 Church, R. B., Hu, K., Magnacca, G. & Cerruti, M. Intercalated Species in Multilayer Graphene Oxide: Insights Gained from In Situ FTIR Spectroscopy with Probe Molecule Delivery. *The Journal of Physical Chemistry C* **120**, 23207-23211 (2016).

6 Cerruti, M., Magnacca, G., Bolis, V. & Morterra, C. Characterization of sol–gel bioglasses with the use of simple model systems: a surface-chemistry approach. *Journal of Materials Chemistry* **13**, 1279-1286 (2003).

7 Jorio, A., Dresselhaus, M., Saito, R. & Dresselhaus, G. (John Wiley & Sons).

8 Eigler, S., Grimm, S., Hof, F. & Hirsch, A. Graphene oxide: a stable carbon framework for functionalization. *Journal of Materials Chemistry A* **1**, 11559-11562 (2013).

9 Eigler, S., Grimm, S. & Hirsch, A. Investigation of the thermal stability of the carbon framework of graphene oxide. *Chemistry–A European Journal* **20**, 984-989 (2014).

10 Englert, J. M. *et al.* Scanning-Raman-microscopy for the statistical analysis of covalently functionalized graphene. *ACS nano* **7**, 5472-5482 (2013).

11 Lucchese, M. M. *et al.* Quantifying ion-induced defects and Raman relaxation length in graphene. *Carbon* **48**, 1592-1597 (2010).

12 Kumar, P. V. *et al.* Scalable enhancement of graphene oxide properties by thermally driven phase transformation. *Nature chemistry* **6**, 151-158 (2014).

13 Yao, B., Chen, J., Huang, L., Zhou, Q. & Shi, G. Base‐Induced Liquid Crystals of Graphene Oxide for Preparing Elastic Graphene Foams with Long‐Range Ordered Microstructures. *Advanced Materials* **28**, 1623-1629 (2016).

14 Li, Y. *et al.* Highly compressible macroporous graphene monoliths via an improved hydrothermal process. *Advanced Materials* **26**, 4789-4793 (2014).

15 Gibson, L. J. & Ashby, M. F. *Cellular solids: structure and properties*. (Cambridge university press, 1999).

16 Gibson, L. J. & Ashby, M. F. in *Proceedings of the Royal Society of London A: Mathematical, Physical and Engineering Sciences.* 43-59 (The Royal Society).
17 Li, J. *et al.* Ultra-light, compressible and fire-resistant graphene aerogel as a highly efficient and recyclable absorbent for organic liquids. *Journal of Materials Chemistry A* **2**, 2934-2941 (2014).
18 Montes-Navajas, P. *et al.* Surface area measurement of graphene oxide in aqueous solutions. *Langmuir* **29**, 13443-13448 (2013).